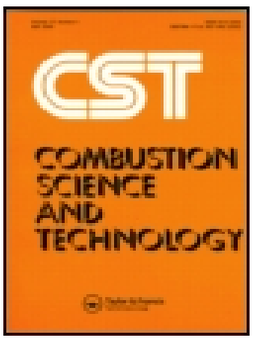

Combustion Science and Technology

ISSN: 0010-2202 (Print) 1563-521X (Online) Journal homepage: https://www.tandfonline.com/loi/gcst20

Preferential Diffusion Effects on the Surface Structure of Turbulent Premixed Hydrogen/Air Flames

M. S. WU , S. KWON , J. F. DRISCOLL & G. M. FAETH

To cite this article: M. S. WU , S. KWON , J. F. DRISCOLL & G. M. FAETH (1991) Preferential Diffusion Effects on the Surface Structure of Turbulent Premixed Hydrogen/Air Flames, Combustion Science and Technology, 78:1-3, 69-96, DOI: 10.1080/00102209108951741

To link to this article: https://doi.org/10.1080/00102209108951741

Published online: 27 Apr 2007.

Combust. Sci. and Tech., 1991, Vol. 78, pp. 69–96
Photocopying permitted by license only

Preferential Diffusion Effects on the Surface Structure of Turbulent Premixed Hydrogen/Air Flames

M. S. WU*, S. KWON, J. F. DRISCOLL and G. M. FAETH *Department of Aerospace Engineering, The University of Michigan, Ann Arbor, Michigan 48109-2140*

(Received August 14, 1990; in final form March 6, 1991)

Abstract—An experimental study of the surface structure of high Reynolds number turbulent premixed hydrogen/air jet flames is reported. Test conditions involved various values of turbulence intensities relative to the laminar flame speed, and stable/neutral/unstable conditions for preferential diffusion, within the wrinkled and mixing-limited thin flamelet regimes. Measurements included laser light sheet imaging to characterize flame surface properties and conditional laser velocimetry to characterize the turbulence properties of the unburned gas. It was found that flame surface area (and thus the local turbulent burning velocity), flame brush thickness and the fractal dimension of the flame surface progressively increased with distance from the flameholder, with maximum values eventually limited by approach to the flame tip. Additionally, the rate of development of these properties with distance from the flameholder increased as turbulence intensities relative to the laminar flame speed increased. Finally, preferential diffusion reduced/increased the rate of increase of these properties for stable/unstable conditions. Taken together, these observations imply that models and correlations of turbulent premixed flame properties for turbulent jet flames must account for effects of flame development, *e.g.*, distance from the flameholder or the point of ignition, and preferential diffusion, in order to adequately characterize flame properties.

NOMENCLATURE

$A_L A_T$	average surface area of time-averaged flame surface, of wrinkled interface
d	burner exit diameter
D_2, D_3	fractal dimension of a contour line, of a surface
$E_i(f)$	temporal power spectral density of velocity component i
f	frequency
l_i	integral length scale based on velocity component i
l_G	Gibson scale
l_k	Kolmogorov scale
L_c	flame length based on a time-averaged reactedness of 0.5
P_L, P_T	perimeter of time-averaged flame surface, of wrinkled interface
r	radial distance
r_f	radial distance to flame surface
Re_d	Reynolds number based on burner exit conditions, $\bar{u}_{o,\text{avg}}\, d/\nu_o$
Re_t	turbulence Reynolds number $\bar{u}'_{o,\text{avg}}\, l_{uo}/\nu_o$
S_L, S_T	laminar and turbulent burning velocity
u	streamwise velocity
v	crosstream velocity
x	streamwise distance
y	azimuthal distance, $rd\theta$

Address Correspondence: G. M. Faeth, 218 Aerospace Engineering, The University of Michigan, Ann Arbor, MI 48109-2140. Telephone: (313) 764-7202; Fax: (313) 763-0578.

Greek Letters

α	thermal diffusivity
δ_L	laminar flame thickness
ε	ruler length for fractal property measurement
θ	azimuthal angle
λ_P	wavelength of flame wrinkles
ν	kinematic viscosity
ρ	density
τ_i	integral time scale based on velocity component i
ϕ	fuel-equivalence ratio

Subscripts

1,2	particular positions
avg	mean burner exit value
c	centerline value
H, V	horizontal and vertical light sheet image
o	burner exit condition

Superscripts

$(^-)$, $(^-)'$	time-average mean and r.m.s. fluctuating property

INTRODUCTION

Turbulent premixed flames have numerous practical applications, *e.g.*, spark-ignition engines, air-breathing propulsion systems, flames and furnaces used in manufacturing and materials processing, and uncontrolled explosions. This has motivated many earlier studies of turbulent premixed flames; however, current understanding is not very complete due to the difficulties of dealing with turbulence/chemistry interactions. Thus, existing correlations of flame properties are characterized by inconsistencies and large scatter even for relatively limited ranges of flame conditions (Abdel-Gayed *et al.* 1976, 1984; Liu and Lenze, 1988; Mantzaras *et al.*, 1989; North and Santavicca, 1990; Williams, 1985). Models of the process also are not highly developed and have had limited experimental evaluation with only marginal success (Bray, 1980; Cant and Bray, 1988; Gouldin, 1987; Libby *et al.*, 1988; Pope, 1990; Wu *et al.*, 1990). Recent work in this laboratory suggests that effects of preferential-diffusion instability may be a factor in the difficulties because this phenomenon can influence flame properties for both stable and unstable conditions—even at the high Reynolds number conditions representative of most practical applications (Wu *et al.*, 1990). The objective of the present investigation was to extend this work to provide information on flame surface properties for stable, neutral and unstable preferential diffusion conditions. Similar to the earlier work, the investigation was limited to premixed turbulent hydrogen/air jet flames operating within the thin flamelet regime defined by Bray (1980).

Within the thin-flamelet regime, preferential diffusion involves the interaction between diffusion of a faster-diffusing reactant and the variation of laminar burning velocity with fuel-equivalence ratio (Manton *et al.*, 1952; Williams, 1985; Joulin and Mitani, 1981). Reactants are consumed within a thin reaction zone; therefore, the faster-diffusing species accumulates near bulges in the flame surface extending toward

the reactants and is depleted from bulges extending toward the products. When the laminar burning velocity increases/decreases with increasing concentration of the fast-diffusing reactant, the bulges grow/decay and the flame is unstable/stable. Hydrogen is the faster diffusing reactant in hydrogen/air flames, and the ratio of the binary diffusivities of hydrogen to oxygen (both with respect to air at room temperature) is roughly 2.3 (Incropera and DeWitt, 1981), while the maximum laminar burning velocity is reached at $\phi = 1.8$ (Andrews and Bradley, 1973). Thus, these flames are unstable/stable for fuel equivalence ratios below/above $\phi = 1.8$.

Clavin and coworkers have studied effects of thermo-diffusive instability, which is closely related to preferential-diffusion instability, using theory and measurements for turbulent flows having large scale and low intensity (Boyer *et al.*, 1980, Clavin and Williams, 1979, 1982; Searby and Clavin, 1986). As noted earlier, Wu *et al.* (1990) also observed preferential-diffusion phenomena in turbulent hydrogen/air jet flames at high Reynolds numbers. In both cases, turbulent distortion of the flame surface was enhanced for unstable conditions and retarded for stable conditions, influencing local turbulent burning velocities accordingly. The latter effect is particularly significant because many practical applications involve heavy hydrocarbons burning in air at fuel-lean conditions, which is in the stable preferential-diffusion regime.

The conditions considered by Clavin and coworkers involved only weak turbulence which is not very representative of practical applications. Wu *et al.* (1990) consider jet flames having more representative turbulence properties; however, only schlieren imaging, which averages properties over a path and is not very quantitative, and point measurements were undertaken. The objective of the present investigation was to complete a more detailed evaluation of effects of preferential diffusion on flame surface properties. This involved analysis of laser light sheet images of the flame surface at various distances from the burner exit, for stable/neutral/unstable preferential-diffusion conditions, and at various values of the relative turbulence intensity, $\bar{u}'/S_L$—the last being measure of the dominance of turbulent mixing on the combustion process. These results were characterized by the flame brush thickness, $\bar{r}_f'$ the ratio of perimeters and areas of the distorted and mean flame surfaces, P_T/P_L and A_T/A_L, the fractal dimension of the flame surface, D_2, and measures of the mean wavelength of flame wrinkles. Additionally, the turbulence characteristics of the unreacted gas were thoroughly characterized using conditional laser velocimetry. Thus, an attempt has been made, in conjunction with the findings of Wu *et al.* (1990), to provide measurements that can be used to help develop models of the turbulent flames subject to preferential diffusion effects, in addition to the direct experimental observations of flame properties under these conditions.

The paper begins with descriptions of experimental methods. Results are then considered treating unburned gas turbulence properties, visualization of the flame surface and flame surface properties in turn. The paper concludes with a discussion of the implications of the measurements for correlations and models of flame properties.

EXPERIMENTAL METHODS

Apparatus

Only a brief description of the premixed burner apparatus will be provided because the arrangement was identical to Wu *et al.* (1990). A coaxial round jet burner was used, with an inner burner having a diameter of 11 mm and a tube length-to-diameter ratio of 50 to yield nearly fully-developed turbulent pipe flow at the burner exit. The

outer burner had a diameter of 58 mm with the outer flame stabilized much like a flat-flame burner above a bed of beads and screens. The burners operated at atmospheric pressure with the combustion products removed through a hood. Instruments were mounted rigidly; therefore, the flame structure was measured by traversing the burner assembly with radial and vertical positioning accuracies of 10 μm and 1 mm, respectively.

All measurements were limited to the jet flame of the inner burner, the outer burner flame only served to provide a hot environment for the jet flame. No attempt was made to match flow properties of the inner and outer burners; rather, the outer burner operated fuel lean ($\phi = 0.3$) with a burner exit velocity of 1 m/s while the inner burner operated at various test conditions. Thus, a mixing layer was present between the combustion product flows of the inner and outer burners. Nevertheless, the mixing layer was observed on schlieren photographs to be well outside the position of the inner jet flame and had negligible influence on its properties (Wu *et al.*, 1990).

Hydrogen (99.95% purity) was supplied from commercial cylinders while dry air (dewpoint less than 240 K) was obtained from laboratory supplies. All gas flow rates were measured with rotameters which were sized to yield maximum uncertainties (95% confidence) of fuel-equivalence ratios less than 5%. The gases were mixed in a manifold and then flowed through lines having length-to-diameter ratios of 400 to achieve uniform mixtures at the burner inlets. Flame arrestor screens were installed in the reactant lines of both burners to control flashback.

Instrumentation

Flame Tomography Measurements were limited to flame surface properties using flame tomography and unburned gas properties using laser velocimetry. Flame tomography involved seeding the unreacted gas with oil drops having a nominal diameter of 1 μm using a TSI 9306 atomizer. Oil drops of this diameter disappear at the flame surface (Boyer *et al.*, 1980). The drops were illuminated by a 200 μm thick laser light sheet created using a Candela pulsed dye laser and two cylindrical lenses. The laser provided 600 mJ of light at 514.5 nm with a 1 μs pulse duration. The scattered laser light was collected using an 85 mm focal length, f1.2 lens and a 35 mm camera back that had its flash synchronization output wired to trigger the laser pulse. Effects of flame radiation were controlled using a 10 nm interference filter in front of the camera lens and a camera shutter duration of 16 ms. Vertical and horizontal light sheet images were obtained by orienting the arrangement accordingly.

The light sheet photographs were enlarged to a 100 × 150 mm format prior to analysis. The enlarged photographs were then digitized using an MTI 65 Vidicon camera and processed using a Gould FD 5000 Image Display and IBM-AT/clone computer. Video camera resolution was the equivalent of 512 × 512 pixels yielding a potential spatial resolution of 140 and 30 μm per pixel for vertical and horizontal light street images. Thus, the 200 μm thickness of the light sheet actually controlled the spatial resolution. Experimental uncertainties of various flame surface properties will be taken up as they are discussed.

Laser Velocity (LV) Unburned gas properties were measured using laser velocimetry. The laser velocimetry system was modified somewhat from Wu *et al.* (1990) in order to provide conditional measurements of unburned gas properties, better spatial resolution, control of directional bias and ambiguity, and additional information concerning turbulence spectra and scales.

A dual-beam laser velocimetry system was used, based on the 488 nm line of a 1 W

TABLE I
Summary of Test Conditions[a]

$\bar{u}'_{o,avg}/S_L$	0.9			2.5		
ϕ	0.8	1.8	3.6	0.8	1.8	3.6
Preferential Diffusion Regime	Unstable	Neutral	Stable	Unstable	Neutral	Stable
$\bar{u}_{o,avg}$ (m/s)	20.4	31.1	20.4	55.0	88.0	58.3
$\bar{u}'_{o,avg}$ (m/s)	2.0	3.1	2.0	5.5	8.8	5.8
S_L (m/s)[b]	2.2	3.5	2.3	2.2	3.5	2.3
ν_o (m^2/s $\times$ 10^6)	19.8	24.7	32.0	19.8	24.7	32.0
α_o(m^2/s $\times$ 10^6)	42.1	60.0	80.9	42.1	60.0	80.9
$Re_d = \bar{u}_{o,avg}\, d/\nu_o$	11300	13900	7000	30600	39200	20000
$Re_t = \bar{u}'_{o,avg}\, l_{uo}/\nu_o$	313	389	194	861	1104	562
L_c/d[c]	2.6	2.6	2.8	4.0	5.3	7.7
l_k (μm)[d]	42	35	60	20	16	27
$\delta_L = \alpha_o/S_L$ (μm)	19	17	35	19	17	35
Flame Regime[e]	Wrinkled, Thin Flamelets			Mixing-Limited, Thin Flamelets		

[a] Round jet burner (d = 11 mm) directed vertically upward with l_{uo} = 3.1 mm. Outer burner flame: ϕ = 0.3, Re_d = 3400 and $\bar{u}_{o,avg}$ = 1 m/s.
[b] Laminar flame speeds from Andrews and Bradley (1973).
[c] Normalized flame length, based on Rayleigh-scattering measurements of Wu *et al.* (1990).
[d] Kolmogorov scale, $l_k = l_{u,o}/(\bar{u}'_{o,avg} l_{u,o}/\nu_o)^{3/4}$, from Tennekes and Lumley (1972).
[e] Based on definitions from Bray (1980).

argon–ion laser. The arrangement had a relatively long focal length (600 mm) transmitting lens because of the relatively large mean velocities (up to 88 m/s). Reasonably good spatial resolution (250 μm long measuring volume) was achieved by observing the probe volume at right angles from the optical axis with 5/4 magnification and a 200 μm aperture in front of the detector. Flame luminousity was controlled using a laser line filter (10 nm bandwidth) in the detector optical path. Frequency shifting was not required for measurements of streamwise velocities because turbulence intensities were less than 15%; however, crosstream (radial) velocities were measured using 40 MHz frequency shifting which was downshifted to convenient frequency ranges for processing.

The seeding particles were oil droplets having a nominal diameter of 1 μm. These particles disappeared at the flame front; therefore, all velocity measurements are conditioned and only represent the properties of the reactants. Data sampling rates always exceeded 100 kHz, which allowed temporal power spectra to be determined up to 50 kHz. Velocity bias was eliminated by sampling the analog output of a commercial burst counter at 100 kHz, using a LeCroy a/d converter (12 bit). Power spectra were found from 64 k samples at each location using an FFT algorithm and an IBM-AT/clone computer. Experimental uncertainties (95% confidence) were dominated by finite sampling times and are estimated to be less than 5% for mean and fluctuating velocities in the streamwise direction and fluctuating velocities in the radial direction.

Test Conditions

Test conditions were within the range considered by Wu *et al.* (1990). Table I is a summary of the properties of the test flames: two values of $\bar{u}'_{o,avg}/S_L$ (0.9 and 2.5) and

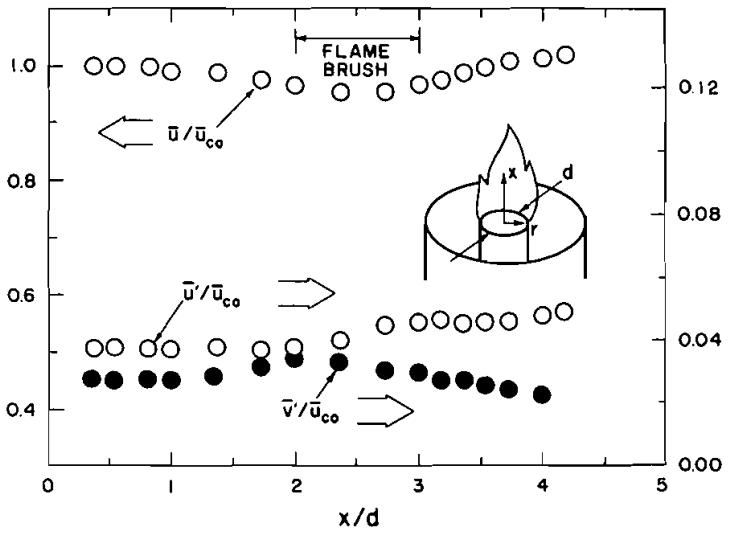

FIGURE 1 Typical mean and fluctuating unburned gas velocities along the flame axis: $\bar{u}'_{o,\mathrm{avg}}/S_L = 0.9$ and $\phi = 1.8$

three fuel-equivalence ratios (0.8, 1.8 and 3.6) were considered. All test conditions are in the thin-flamelet regime defined by Bray (1980), with the lower and higher values of $\bar{u}'_{o,\mathrm{avg}}/S_L$ placing the flames in the wrinkled and mixing-limited thin flamelet regimes, respectively. In particular, flames with $\bar{u}'_{o,\mathrm{avg}}/S_L = 2.5$ are more likely to have local islands of reactants than those having $\bar{u}'_{o,\mathrm{avg}}/S_L = 0.9$, although both have wrinkled continuous flame sheets (Bray, 1980). The three values of ϕ vary flame conditions with respect to preferential-diffusion instability: $\phi = 0.8$, 1.8 and 3.6 being in the unstable, neutral and stable regimes, respectively. In addition, $\phi = 0.8$ and 3.6 have nearly the same laminar flame speeds (Andrews and Bradley, 1973) and burner exit conditions so that observed differences in flame surface properties between these two flames can be attributed to effects of preferential diffusion for each $\bar{u}'_{o,\mathrm{avg}}/S_L$.

The values of $\bar{u}_{o,\mathrm{avg}}$, $\bar{u}'_{o,\mathrm{avg}}$ and $l_{u,o}$ in Table I were determined from the LV measurements, the last involving use of Taylor's hypothesis (Hinze, 1975). Burner exit and turbulence Reynolds numbers were in the range 7000–40000 and 200–1100, which includes the same range as Wu *et al.* (1990). Flame lengths, L_c, are taken as the condition where time-averaged unreactedness along the axis was 0.5, from the Rayleigh-scattering measurements of Wu *et al.* (1990). Flame lengths are in the range $L_c/d = 2.6$–7.7 which implies that the unreacted gas is largely within the potential core of the jet. The Kolmogorov scales, l_k, were estimated as $l_{u,o}/(\bar{u}'_{o,\mathrm{avg}} l_{u,o}/\nu_o)^{3/4}$ from Tennekes and Lumley (1972): they are generally comparable or larger than the flame thickness which is representative of the thin flamelet regime.

RESULTS AND DISCUSSION

Unburned Gas Properties

Mean and Fluctuating Velocities The turbulent flow field properties of the unreacted gas were quantified in detail. Figure 1 is an illustration of conditional mean and fluctuating velocities long the axis for $\bar{u}'_{o,\mathrm{avg}}/S_L = 0.9$ and $\phi = 1.8$. Findings for other

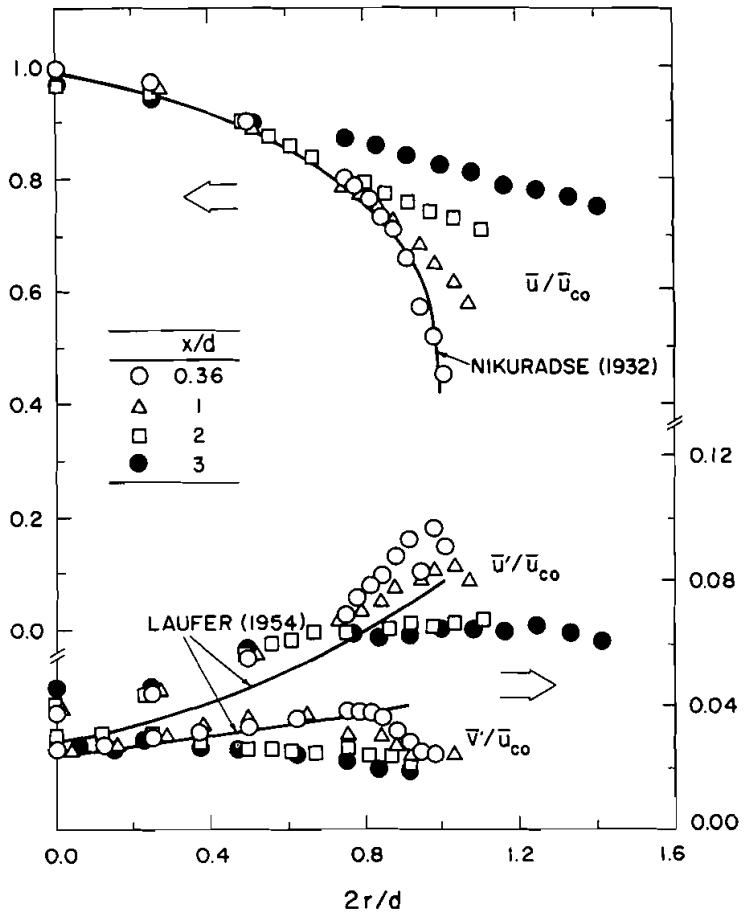

FIGURE 2 Typical radial profiles of mean and fluctuating unburned gas velocities: $\tilde{u}'_{o,avg}/S_L = 0.9$ and $\phi = 1.8$

conditions were similar, see Wu *et al.* (1990) for some typical examples of unconditioned velocities along the axis. The limits of flame position along the axis, which define the region of the flame brush, are also shown on the plot for reference purposes. Typical of flows within a potential core region, the unreacted gas exhibits only modest variations of mean and fluctuating velocities. Additionally, Wu *et al.* (1990) point out that the potential core is unusually long for present flows, extending up to $x/d = 10$ (for a decay of mean velocities less than 10%) because the immediate surroundings are the low-density gaseous combustion products of the outer burner flame which reduces entrainment rates.

Radial variations of mean and fluctuating velocities, for the same conditions as Figure 1, are illustrated in Figure 2 for x/d in the range 0.36–3; however, findings for $x/d = 0.18$, which was the position closest to the burner exit that could be accessed by laser velocimetry, can be found in Wu *et al.* (1990). Properties near the burner exit, $x/d = 0.18$ and 0.36, approximate the mean and fluctuating velocities of fully-turbulent pipe flow from Nikuradse (1932) and Laufer (1954). With increasing distance from the burner, however, the wake-like flow due to the pressure of the

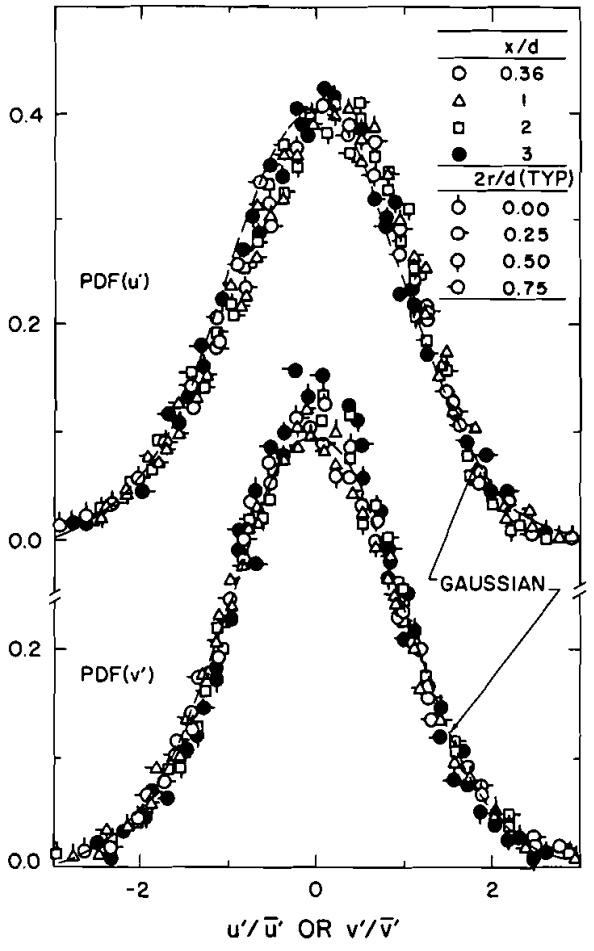

FIGURE 3 PDF's of streamwise and crosstream unburned gas velocities: $\bar{u}'_{o,\text{avg}}/S_L = 0.9$ and $\phi = 1.8$.

burner passage walls decays and flow properties become more uniform. In general, the flow is anisotropic with $\bar{u}'/\bar{v}'$ in the range 1.2–3.0, except for the region very near the passage walls where the degree of anisotropy is even larger.

Normalized probability density functions (PDF's) of streamwise and crosstream velocity functions for various points within the unreacted gas are plotted in Figure 3. These results are for the same flame as Figures 1 and 2, however, they are typical of other conditions. In spite of the anisotropy, the velocity fluctuations are seen to approximate Gaussian functions, which is characteristic of most turbulent shear flows (Hinze, 1975). A possible exception is a slight positive skewness of the streamwise velocity fluctuations but this is not felt to be significant in comparison to experimental uncertainties.

Spectra and Integral Scales Conditional temporal power spectra of streamwise and crosstream velocity fluctuations for various streamwise and radial positions are plotted in Figures 4 and 5. These results also correspond to the flame considered in Figures 1 to 3. The present integral time scales, τ_u or τ_v, are defined by Hinze (1975)

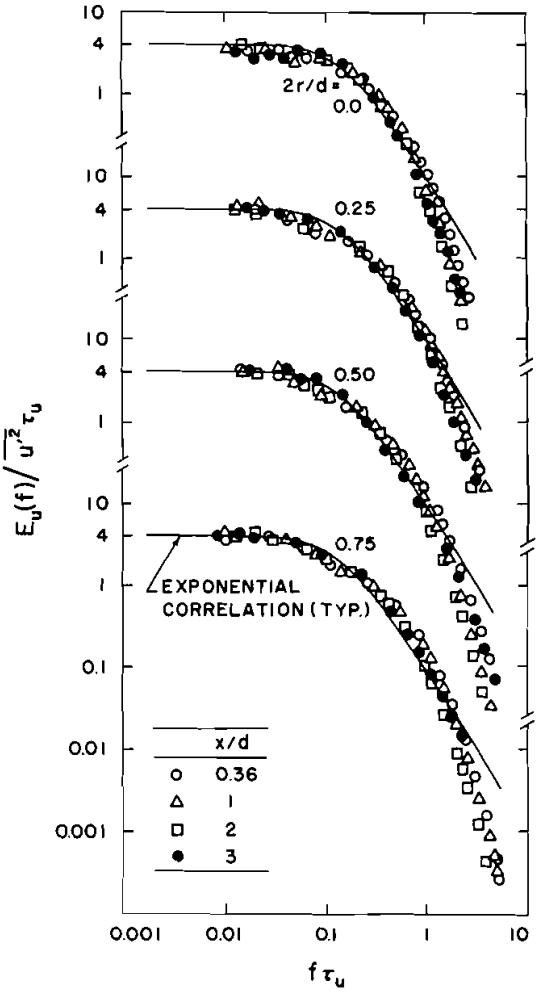

FIGURE 4 Temporal power spectra of streamwise unburned gas velocity fluctuations: $\tilde{u}'_{o,avg}/S_L = 0.9$ and $\phi = 1.8$

as the ordinate intercepts of the power spectra, $E_u(0)$ or $E_v(0)$, divided by $4\tilde{u}'^2$ or $4\tilde{v}'^2$. Thus, after normalization, the spectra of Figures 4 and 5 have an ordinate intercept of 4.0. Also shown on the plots are the power spectra when the autocorrelations are decaying exponential functions, *i.e.*, when the power spectra are $4/(1 + (2\pi f\tau_{u \text{ or } v})^2)$. Except for the highest frequencies, where Kolmogorov scales are approached, the normalized streamwise power spectra illustrated in Figure 4 approximate the behavior of the exponential autocorrelation functions. Most of the normalized crosstream power spectra illustrated in Figure 5 also approximate the behavior of exponential autocorrelation functions as well. However, spectra near the axis and near the burner exit display a local maximum that is not observed elsewhere. Laufer (1954) measured similar spectra for transverse velocity fluctuations in turbulent pipe flows so that the effect is due to the origin of the flow. The reason for this behavior is that conservation of mass requires that spectra of transverse velocity fluctuations have a portion that

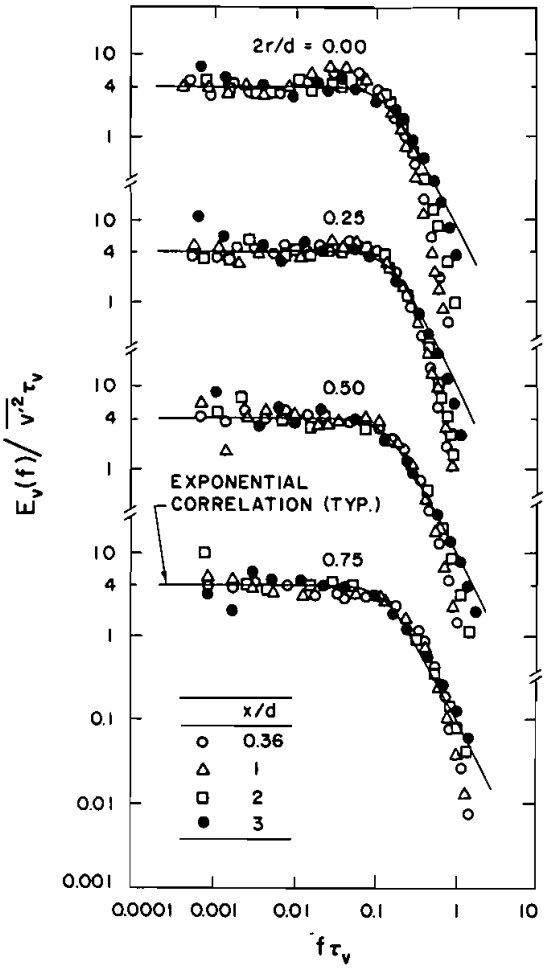

FIGURE 5 Temporal power spectra of crosstream unburned gas velocity fluctuations: $\bar{u}'_{o,\text{avg}}/S_L = 0.9$ and $\phi = 1.8$.

becomes negative, resembling a Frenkiel function rather than an exponential function, with a corresponding peak in the temporal spectrum (Tennekes and Lumley, 1972). This feature decays rapidly, however, so that exponential autocorrelations, which simplify stochastic simulations of the flow field (Box and Jenkins, 1976), would be a reasonable approximation for most of the flow.

The temporal integral scales, τ_u and τ_v, are plotted in Figure 6 for positions corresponding to the spectra of Figure 5. The streamwise integral length scale, l_u is also shown on the plots. The length scales were found from the measured integral time scales and local mean velocities using Taylor's hypothesis, *e.g.*, $l_u = \bar{u}\tau_u$. It was found that l_u was 4 ± 1 mm at all 16 axial and radial locations where measurements were made. This value is consistent with Laufer's (1954) measurements which indicate $l_u \approx 0.4d$ or roughly 4 mm for present measurements. The integral time scale, τ_u, exhibits a greater variation than l_u within the unreacted gas, largely through the variation of mean velocities seen in Figure 2 as reflected by Taylor's hypothesis. The

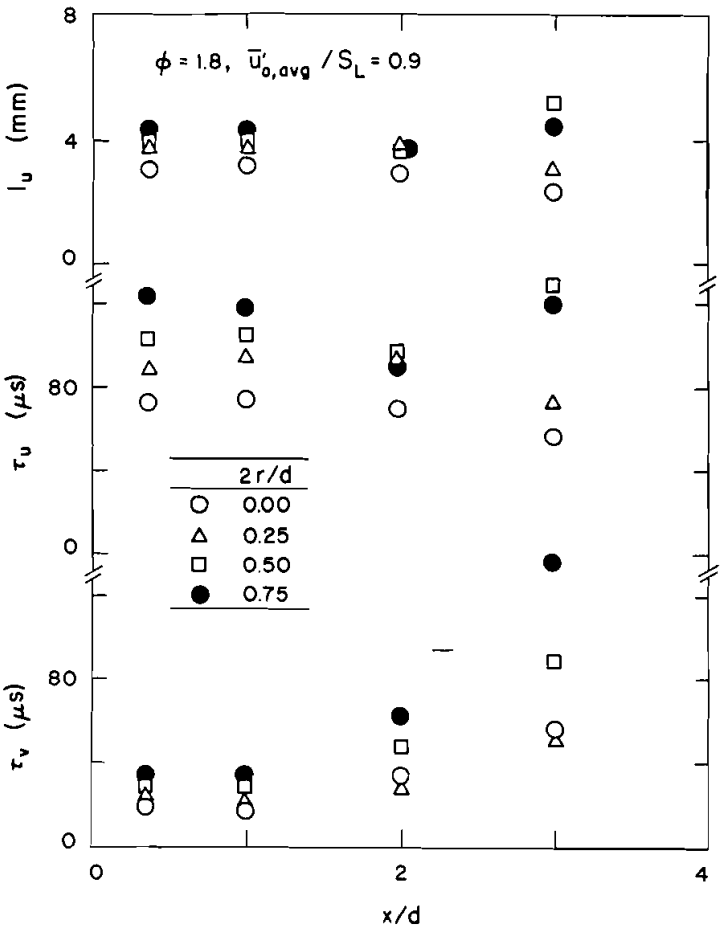

FIGURE 6 Integral length and time scales of streamwise and crosstream unburned gas velocity fluctuations: $\bar{u}'_{o,avg}/S_L = 0.9$ and $\phi = 1.8$.

integral time scale, τ_v, is generally less than τ_u because the autocorrelation function for $\bar{v}'$ has a negative portion whereas the autocorrelation for $\bar{u}'$ approximates an exponential function (Tennekes and Lumley, 1972).

Flame Surface Properties

Light Sheet Images Typical light sheet images for vertical planes through the axis appear in Figures 7 and 8 for $\bar{u}'_{o,avg}/S_L = 0.9$ and 2.5. Note that the quality of these tomographs is much poorer than those that were analyzed because a large field of view was used to cover the entire flame height in a few images. Each figure includes results for unstable, neutral and stable fuel equivalence ratios, along with $l_{u,o}$ as a measure of turbulent length scales. The results show that the flame structure varies with height above the burner, $\bar{u}'_{o,avg}/S_L$ and preferential diffusion regime. First of all, the extent of wrinkling and lateral deflection of the flame surfaces increases progressively with height above the burner. This follows because time, or equivalently distance, is required for the random motion of the turbulent field to deflect the flame laterally

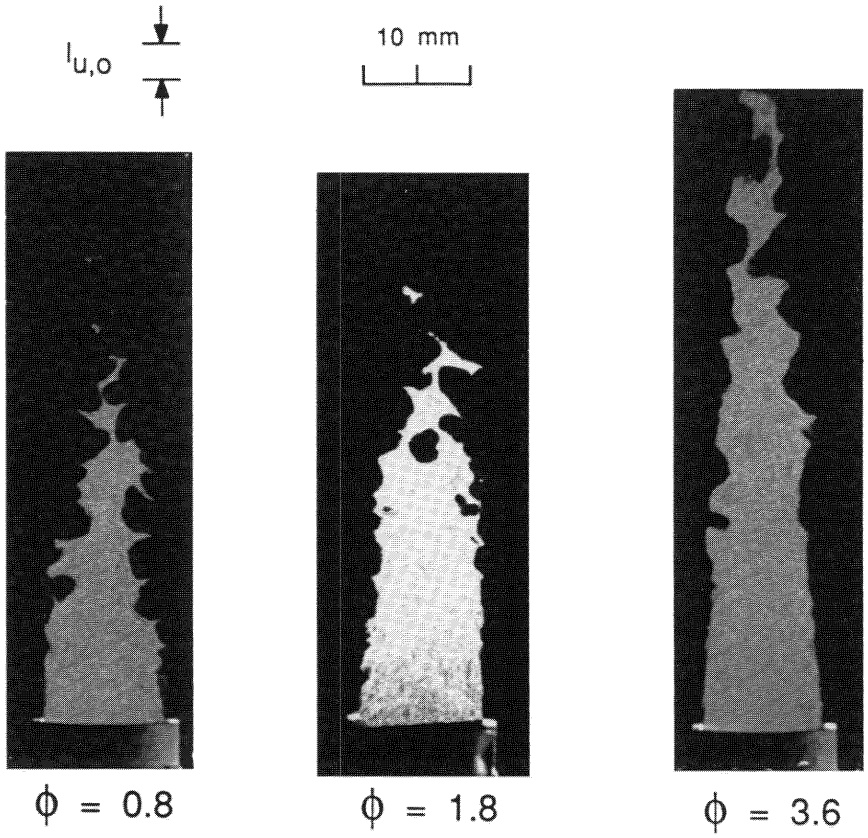

FIGURE 7 Typical light sheet photographs for a vertical plane through the flame axis: $\bar{u}'_{o,\mathrm{avg}}/S_L = 0.9$.

from the points of attachment at its base. This behavior is analogous to the progressively increasing lateral spread of fluid particles with distance from their source due to turbulent dispersion (Hinze, 1975).

Increasing the relative turbulence intensity, $\bar{u}'_{o,\mathrm{avg}}/S_L$, causes both the flame length and degree of distortion of the flame surface to increase, compare Figures 7 and 8. The increased flame length follows from the nature of the present experiments where increased $\bar{u}'_{o,\mathrm{avg}}/S_L$ is accompanied by increased $\bar{u}_{o,\mathrm{avg}}/S_L$ because the turbulence intensity at the burner exit, $\bar{u}'_{o,\mathrm{avg}}/\bar{u}_{o,\mathrm{avg}}$, is nearly constant over the test range. Then low values of relative turbulence intensities imply only small increases of the effective turbulent burning velocity from the laminar burning velocity so that the angle of the flames to the mean flow direction must decrease with increasing mean velocities—increasing the flame length. This behavior continues until $\bar{u}'_{o,\mathrm{avg}}/S_L$ becomes large, *ca.* 10, where mixing-limited combustion is achieved and the flame length is relatively independent of the mean burner exit velocity (Bray, 1980; Wu *et al.*, 1990).

Comparing Figures 7 and 8 shows that a much finer grained flame surface structure is created as $\bar{u}'_{o,\mathrm{avg}}/S_L$ is increased. Peters (1986) discusses this behavior in terms of the Gibson scale, l_G, which is the scale of vortices that have circumferential velocities comparable to the laminar burning velocity. Because both circumferential velocities and times of propagation across vortex elements decrease with decreasing vortex size,

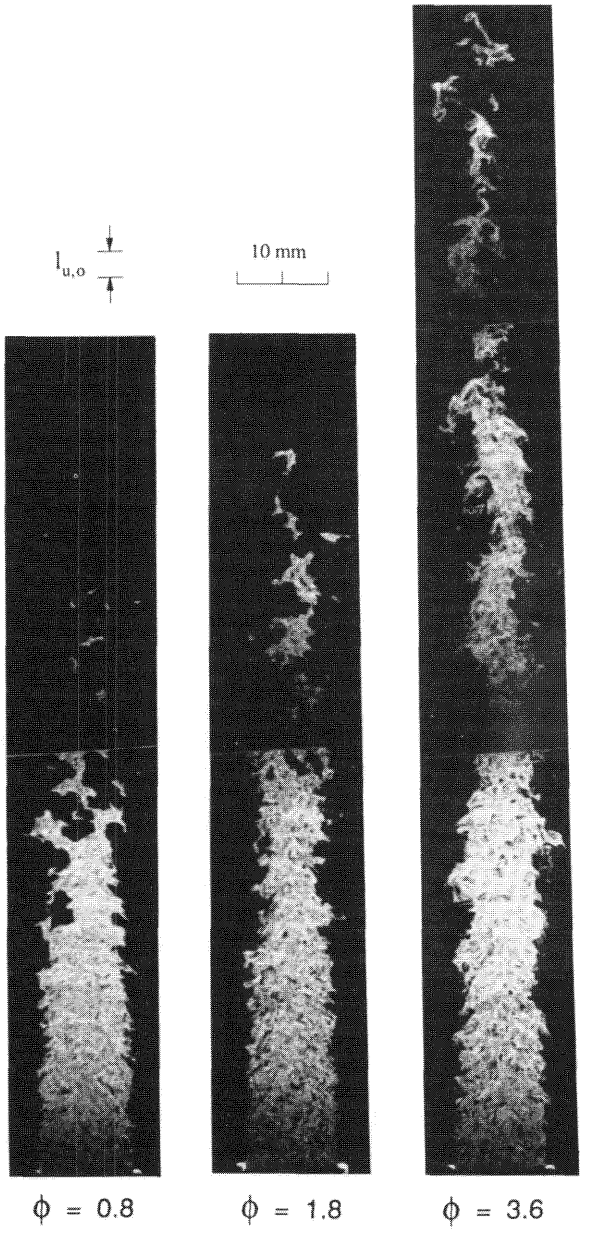

FIGURE 8 Typical light sheet photographs for vertical plane through the flame axis: $\bar{u}'_{o,\mathrm{avg}}/S_L = 2.5$.

the Gibson scale is a measure of the smallest vortices that can appreciably deflect the flame surface. Peters (1986) suggests that $l_G = l_{u,o}\ (S_L/\bar{u}'_{o,\mathrm{avg}})^3$ for $\bar{u}'_{o,\mathrm{avg}}/S_L > 1$, assuming that burner exit conditions are representative of the flame as a whole, yielding $l_G = 200\ \mu$m for $\bar{u}'_{o,\mathrm{avg}}/S_L = 2.5$. Similar considerations suggest that l_G is of the same order of magnitude as spatial integral scales, 3–4 mm, for $\bar{u}'_{o,\mathrm{avg}}/S_L = 0.9$. Based on these ideas, the finer grained flame structure for $\bar{u}'_{o,\mathrm{avg}}/S_L = 2.5$ than 0.9 is not surprising.

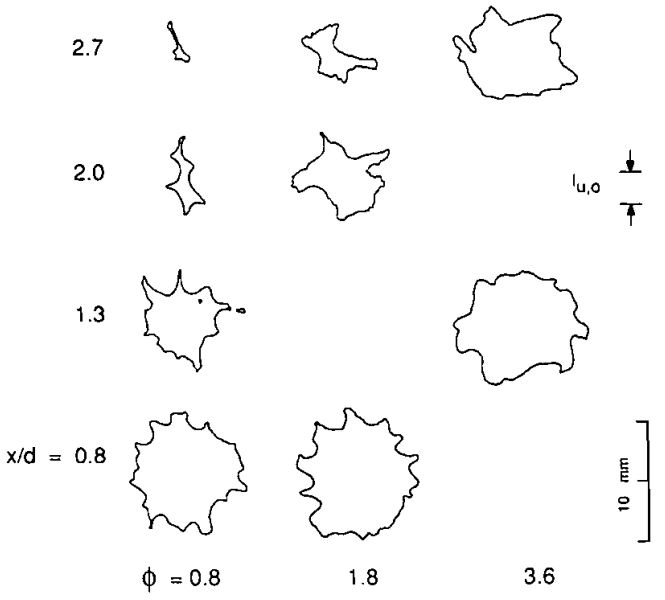

FIGURE 9 Typical light sheet images for horizontal planes at various heights above the burner: $\bar{u}'_{o,avg}/S_L = 0.9$.

The third main effect seen in Figures 7 and 8 relates to preferential diffusion. In particular, differences between the flames at $\phi = 0.8$ and 3.6 for each value of relative turbulence intensity can be attributed to preferential diffusion because these flames are otherwise nearly identical, *i.e.*, they have nearly the same values of $\bar{u}_{o,avg}$, $\bar{u}'_{o,avg}$ and S_L (see Table I). The effect of preferential diffusion is clearly quite pronounced even at the relatively high Reynolds numbers of the present tests; the unstable ($\phi = 0.8$) flames are significantly shorter and have higher levels of surface distortion at a given distance from the burner exit than the stable ($\phi = 3.6$) flames. This provides direct evidence that the mechanism of preferential diffusion is acting to either enhance or retard turbulent distortion of the flame surface for unstable or stable conditions. Naturally, effects of increasing distortion with increasing distance from the burner exit still act; thus, while the stable flames have less distortion than the unstable flames at a given height above the burner exit, the stable flames still exhibit significant degrees of distortion near their tips which are much farther from the burner exit than those of the unstable flames. The neutral ($\phi = 1.8$) flames have behavior somewhat intermediate between the unstable and stable flames with respect to flame length and surface distortion for present test conditions. This comes about due to complex interactions between the initial conditions and S_L, the presence or absence of preferential diffusion effects, and the distance from the burner because $\bar{u}_{o,avg}$, $u'_{o,avg}$ and S_L are roughly 50% larger for $\phi = 1.8$ than for $\phi = 0.8$ or 3.6.

Some typical light sheet images for horizontal planes at various heights above the burner appear in Figures 9 and 10. Values of relative turbulence intensity and ϕ for these figures are the same as Figures 7 and 8. The region considered is toward the base of the longest flames, $x/d \leqslant 4$, so that results for all three values of ϕ can be compared. The general features of these results are similar to the vertical light sheet photographs of Figures 7 and 8: the degree of surface distortion increases with increasing height above the burner, the degree of fine-grained roughness of the flame

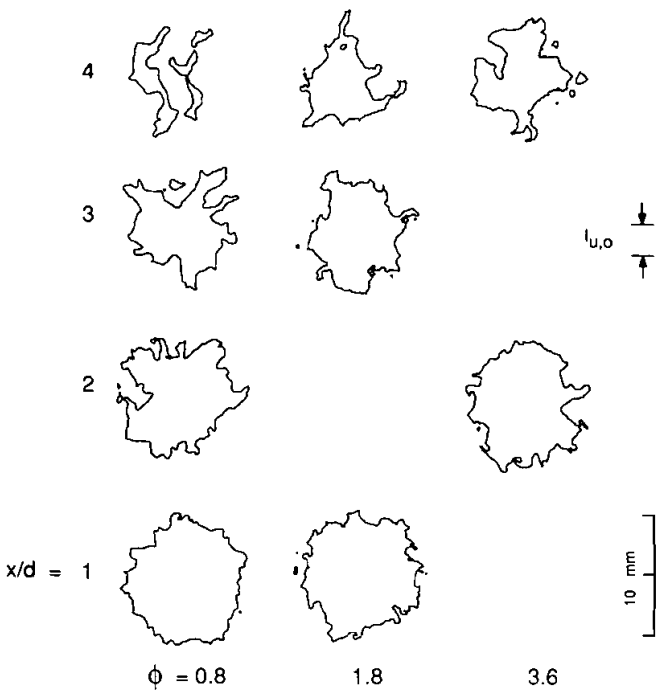

FIGURE 10 Typical light sheet images for horizontal planes at various heights above the burner: $\bar{u}'_{o,\text{avg}}/S_L = 2.5$.

surface increases with increasing $\bar{u}'_{o,\text{avg}}/S_L$, and the distortion of the flame surface at a particular x/d is greater for unstable ($\phi = 0.8$) than for stable ($\phi = 3.6$) preferential diffusion conditions even though, other properties of these flames are the same.

Flame Position Mean flame positions, $\bar{r}_f$, and the r.m.s. fluctuation of flame position or flame brush thickness, $\bar{r}'_f$, are plotted as a function of height above the burner in Figures 11 and 12 for $\bar{u}'_{o,\text{avg}}/S_L = 0.9$ and 2.5. These results were obtained by ensemble-averaging 12–20 digitized light sheet images in the vertical plane at each spatial location. Experimental uncertainties (95% confidence) of these measurements are less than 5% for $\bar{r}_f$, and 15% for $\bar{r}'_f$.

Mean flame positions in Figures 11 and 12 monotonically decay toward the flame axis from the burner exit. Thus, the flame zone was generally well inside the position of the mixing layer between the inner and outer burner flows which was located at $r/d > 0.5$—aside from the region near the point of flame attachment. The development of flame distortion with distance from the burner exit can be seen from the rapid increase of $\bar{r}'_f/d$ near the burner exit. However, the boundary conditions also require that the flames have a finite length so that after reaching a maximum value $\bar{r}'_f/d$ begins to decline again toward the flame tip—this is particularly evident for $\bar{u}'_{o,\text{avg}}/S_L = 0.9$ and $\phi = 1.8$.

Effects of preferential diffusion also can be seen in Figures 11 and 12. As discussed earlier, unstable ($\phi = 0.8$) and stable ($\phi = 3.6$) conditions increase and decrease turbulent distortion of the flame surface. This is reflected by an increased rate of reduction of mean flame radius and larger maximum values of the flame brush thickness near the burner exit for unstable than for stable conditions. However, the

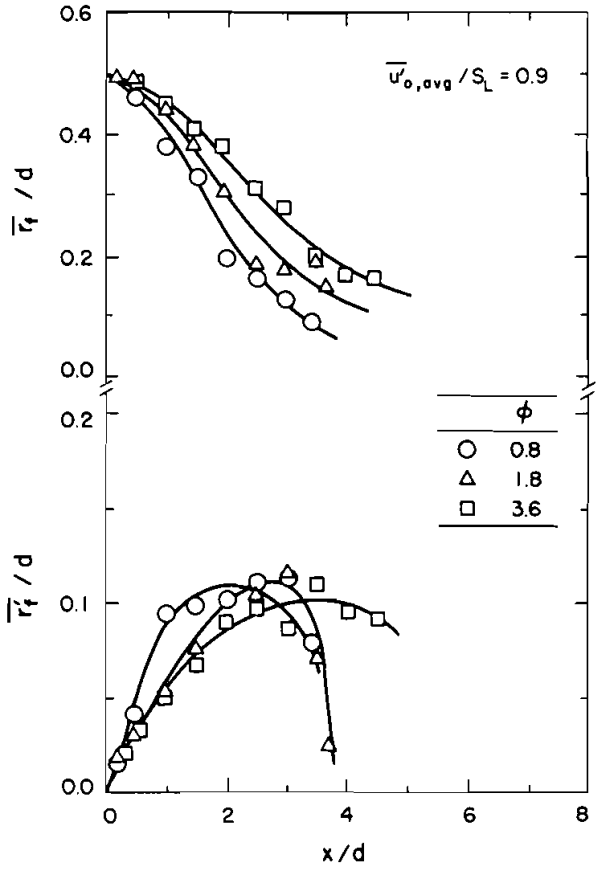

FIGURE 11 Mean and fluctuating radial flame position as a function of height above the burner: $\bar{u}'_{o,avg}/S_L = 0.9$.

progressive increase of flame surface distortion with distance from the burner exit counteracts effects of preferential diffusion somewhat for the longer flames at stable conditions, *i.e.*, at larger x/d, $\bar{r}'_f/d$ is actualy largest for the stable flame. Differences between stable and unstable conditions, however, tend to become smaller as $\bar{u}'_{o,avg}/S_L$ increases—particularly in the region near the burner exit. As noted earlier, properties of the neutral flames tend to be intermediate of the unstable and stable flames but this is somewhat fortuitous because the operating conditions for the neutral flame differ appreciably from the other two at each value of $\bar{u}'_{o,avg}/S_L$.

Flame Perimeter and Area A measure of the distortion fo the flame surface was found by measuring the perimeters of the flame surfaces on the vertical and horizontal light sheet images. For the vertical light sheet images, the flame length was divided into segments having a length of $0.7\,d$ and the perimeter of the wrinkled surface, P_{TV}, and the ensemble-averaged perimeter of the mean flame position, P_{LV}, were found for each segment. For the horizontal light sheet images, the perimeter of the wrinkled surface, P_{TH}, can be found directly while P_{LH} was taken to be the perimeter of a circle having the same area as the flame image. Flame surface distortions as small as the Gibson scale for $\bar{u}'_{o,avg}/S_L = 2.5$ could be resolved (roughly 200 μm). In view of this,

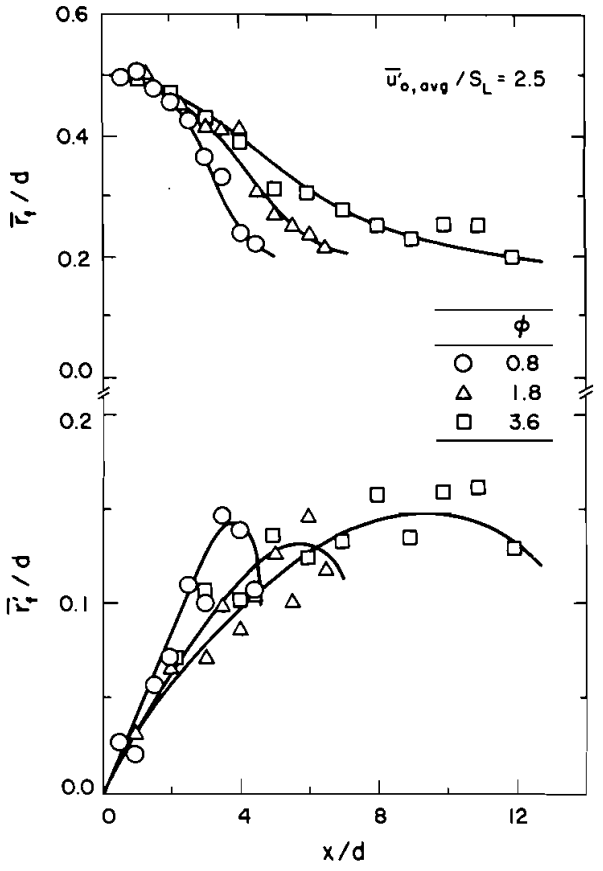

FIGURE 12 Mean and fluctuating radial flame position as a function of height above the burner: $\bar{u}'_{o,avg}/S_L = 2.5$.

and findings to be discussed in connection with fractal properties, effects of filtering of fine scale features by limited resolution were not very significant. Accounting for potential filtering, experimental uncertainties (95% confidence) of P_{TV}/P_{LV} and P_{TH}/P_{LH} were estimated to be less than 10 and 20% for $\bar{u}'_{o,avg}/S_L = 0.9$ and 2.5.

The variations of P_{TV}/P_{LV} and P_{TH}/P_{LH} are plotted as a function of distance from the burner in Figure 13. Unlike the flame brush thickness, the perimeter ratios increase monotonically with increasing distance from the flameholder. Effects of preferential diffusion can also be seen, with the perimeter ratios for unstable ($\phi = 0.8$) conditions being consistently larger than those of stable ($\phi = 3.6$) conditions at a given distance from the burner exit, even though turbulence properties and laminar flame speeds are nearly identical. However, effects of preferential diffusion are clearly smaller for the larger value of relative turbulence intensity. This is reasonable because effects of passive turbulent distortion are more dominant than active preferential diffusion flame propagation relative to the velocity field when relative turbulence intensities are large. Another interesting feature of these results is that perimeter ratios in the vertical and horizontal directions are nearly the same for unstable ($\phi = 0.8$) conditions but the vertical are larger than the horizontal perimeter

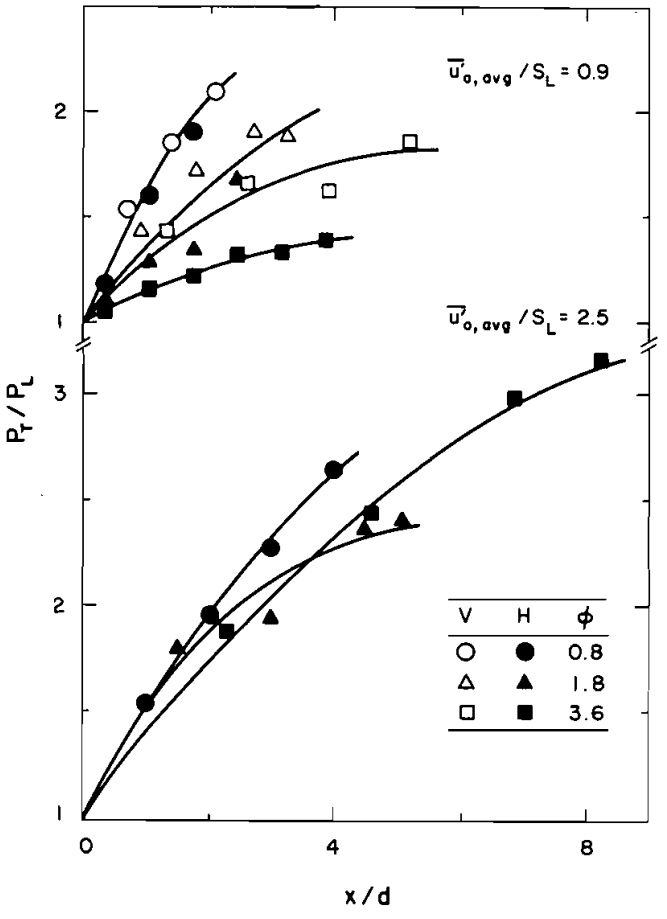

FIGURE 13 P_T/P_L as a function of height above the burner for vertical (V) and horizontal (H) planes.

ratios for stable ($\phi = 3.6$) conditions. This suggests that the enhanced distortion at unstable conditions tends to be more isotropic because much of it is generated by the flame itself, while reduced levels of distortion for stable conditions tend to reflect the underlying anisotropy of the turbulent field of the unburned gas to a greater degree.

The average surface area of the wrinkled interface, A_T, was determined from the perimeters of the horizontal and vertical light sheet images using the exact definitions of perimeter and surface area:

$$P_{TV} = \int_{x_1}^{x_2} (1 + (\partial r_f/\partial x)^2)^{1/2}\, dx, \tag{1}$$

$$P_{TH} = \int_{0}^{2\pi\bar{r}_f} (1 + (\partial r_f/\partial y)^2)^{1/2}\, dy, \tag{2}$$

$$A_T = \int_{x_1}^{x_2} \int_{0}^{2\pi\bar{r}_f} (1 + (\partial r_f/\partial x)^2 + (\partial r_f/\partial y)^2)^{1/2}\, dy dx, \tag{3}$$

where r_f is the radial location of the flame surface, x is the streamwise coordinate and y is the azimuthal coordinate, $\bar{r}_f d\theta$, in this cylindrical coordinate system. A simple closed-form expression relating A_T, P_{TV} and P_{TH} can be derived if the derivatives $\partial r_f/\partial x$ and $\partial r_f/\partial y$ are sufficiently small; then the kernals of the integrals in Eqs. (1) and (2) become $(1 + (\partial r_f/\partial x)^2/2)$ and $(1 + (\partial r_f/\partial y)^2/2)$ so that Eq. (3) can be approximated as

$$A_T/A_L = (P_{TV}/P_{LV}) + (P_{TH}/P_{LH}) - 1. \quad (4)$$

Equation (4) is not exact for large amplitude wrinkles; however, the uncertainty of the approximation can be estimated by evaluating both sides for a wavy sinusoidal surface $z = z_o \sin(2\pi x_1/\lambda_1) \sin(2\pi x_2/\lambda_2)$. For wrinkles having amplitude-to-wavelength ratios (z_o/λ) less than 5, the approximation is correct within 10%. All wrinkles that were observed met this criterion so that Eq. (4) was used to evaluate A_T/A_L for the present flames. Then in view of the uncertainties of the perimeter ratios, the experimental uncertainties (95% confidence) of A_T/A_L are estimated to be less than 20 and 30% for $\bar{u}'_{o,\text{avg}}/S_L = 0.9$ and 2.5.

The flame surface area ratios, A_T/A_L, are plotted as a function of height above the burner in Figure 14. Similar to the perimeter ratios, A_T/A_L increases with increasing height above the burner. To the extent that A_T/A_L is a measure of the local turbulent burning velocity, which is most appropriate for neutral conditions for preferential diffusion and modest stretch rates (Gouldin, 1987), this means that the use of effective turbulent burning velocities for jet flames, based on an average taken over the flame surface (Ballal, 1979; Dandekar and Gouldin, 1982; Grover *et al.*, 1959; Wu *et al.*, 1990), provides a measure of effects of turbulence on flame speeds but tends to obscure important effects of distance from the point of flame attachment.

Similar to the perimeter ratios, the area ratios illustrated in Figure 14 exhibit effects of preferential diffusion by comparing results for unstable ($\phi = 0.8$) and stable ($\phi = 3.6$) conditions. The unstable flame generally has a larger value of A_T/A_L at a given distance from the burner exit; however, differences between unstable and stable conditions decrease as the relative turbulence intensity increases for the reasons discussed earlier. The effect of the growth of the flame surface distortions with distance plays a role as well; for example, the stable flames extend farther than the rest due to lower levels of distortion near the burner, but eventually at large distances from the burner exit actually exhibit higher values of A_T/A_L than the other flame conditions.

Assuming that S_T/S_L is primarily controlled by the distortion of the flame surface as represented by A_T/A_L, the results illustrated in Figure 14 can be related to other observations of effects of preferential diffusion. In particular, Wu *et al.* (1990) find two branches for S_T/S_L averaged over the entire length of turbulent jet flames when plotted as a function of $\bar{u}'_{o,\text{avg}}/S_L$: a stable branch and a neutral/unstable branch, the latter exhibiting a faster rate of increase with $\bar{u}'_{o,\text{avg}}/S_L$. Similarly, observations of Abdel-Gayed *et al.* (1976, 1984) for turbulent hydrogen/air flames and Liu and Lenze (1988) for turbulent hydrogen/methane/air flames exhibited faster growth rates of S_T/S_L with increasing $\bar{u}'_{o,\text{avg}}/S_L$ for neutral/unstable conditions than for stable conditions. The results illustrated in Figure 14 generally agree with these trends, but also suggest effects of distance from the burner exit on S_T/S_L at various $\bar{u}'_{o,\text{avg}}/S_L$ as well as greater differences between results for neutral and unstable conditions.

Fractal Properties A popular measure of the degree of wrinkledness of flame surfaces is the fractal dimension, D_2 (Gouldin, 1987; Gouldin *et al.*, 1988; Mantzaras *et*

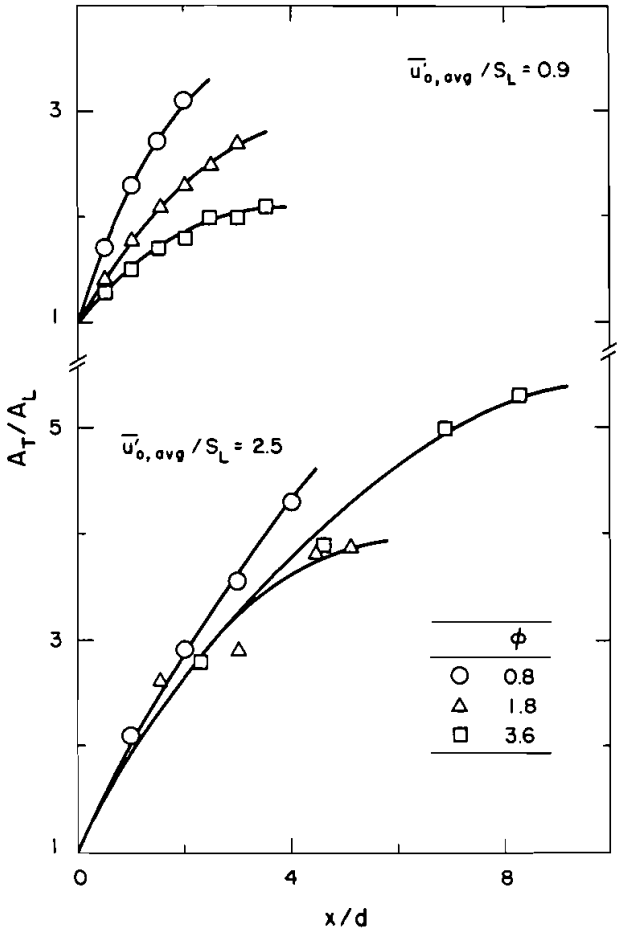

FIGURE 14 A_T/A_L as a function of height above the burner.

al. 1989; Murayama and Takeno, 1988; North and Santavicca, 1990; Santavicca *et al.*, 1990; Videto and Santavicca, 1990). D_2 was found for the present flames by measuring values of the flame perimeter using rulers of different size, ε, as discussed by Mandelbrot (1982). Beginning with one location on the interface, a computer routine was used to find the locus of points on an arc of radius ε about that location. The point where the arc intersects the interface determines the next location where the arc is to be centered, etc., until the extent of the surface has been reached. If the arc intersects the interface at more than one location, the next center is taken to be the nearest intersection along the interface. The flame perimeter associated with a given value of ε is the number of arcs drawn, multiplied by the radius (ε) of each.

A typical plot of normalized perimeter as a function of normalized ruler size is illustrated in Figure 15. These measurements are for horizontal light sheet images at $x/d = 6.9$, $\tilde{u}'_{o,avg}/S_L = 2.5$ and $\phi = 3.6$, ensemble-averaging results for each ruler size over 12 images in order to smooth the plot. The plot approaches two limits: at small ε where the complete perimeter is resolved, and at large ε where ruler sizes approach the maximum dimension of the flame perimeter so that round-off of the procedure causes the perimeter to vary in an irregular manner. Between these limits,

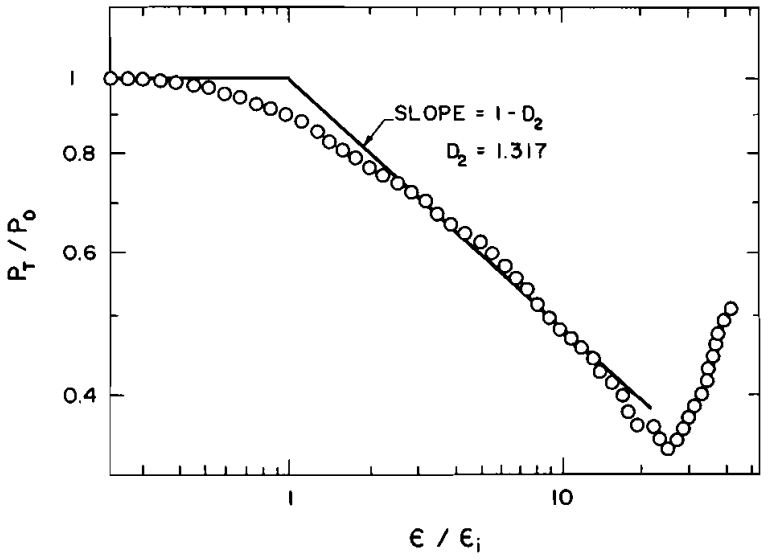

FIGURE 15 Sample determination of D_2 for a horizontal plane: $\bar{u}'_{o,avg}/S_L = 2.5$, $\phi = 3.6$ and $x/d = 6.9$.

the curve exhibits a relatively smooth slope that is suggestive of fractal-like behavior. The slope of the best-fit linear curve for this intermediate region is $1\text{-}D_2$, assuming that the flame surface is fractal (Mandelbrot, 1982). Estimated experimental uncertainties (95% confidence) are less than 20% for D_2-1. In order to compare present results with other work, where the assumption of isotropic surface properties is generally invoked (Gouldin, 1987; Lovejoy, 1982; Mantzaras *et al.*, 1989; North and Santavicca, 1990; Sreenivasan and Meneveau, 1986), it will be assumed that $D_3 = 1 + D_2$ (Mandelbrot, 1982), in the following.

In Figure 15, the intersections between the linear fit and the small and large scale limits define inner and outer cut-offs that are representative of the small and large scale irregularities of the flame surface (Gouldin, 1987). Present outer scales were simply comparable to the largest dimensions of the flame perimeter while inner scales were marginally resolvable at $\bar{u}'_{o,avg}/S_L = 2.5$; therefore, cut-offs are not reported in the following. However, behavior near the inner cut-off provides insight concerning the resolution of flame surface perimeters. In particular, results of Figure 15 are for $\bar{u}'_{o,avg}/S_L = 2.5$ with a very irregular surface that yielded a large fractal dimension. Even at this condition, however, the variation of P_T/P_O is gradual near the inner cut-off ($\varepsilon/\varepsilon_i = 1$). Applying fractal relationships for the variation of P_T with ε (Gouldin, 1987), between the inner cut-off and the Gibson scale, yields potential underestimation of P_T less than 10% (at least to the extent that the Gibson scale represents the smallest surface distortions). This is representative of results at $\bar{u}'_{o,avg}/S_L = 2.5$, while similar considerations suggest negligible resolution errors for results at $\bar{u}'_{o,avg}/S_L = 0.9$.

Values of D_2 as a function of height above the burner are plotted for all six flames tested in Figure 16. These results were obtained using horizontal light sheet images in order to provide results at well-defined distances from the burner exit: the range $x/d = 1$ up to the region of the flame tip was considered. Values of D_2 are seen to be influenced by height above the burner, $\bar{u}'_{o,avg}/S_L$ and effects of preferential diffusion instability, similar to the normalized flame area. For all conditions, D_2 progressively

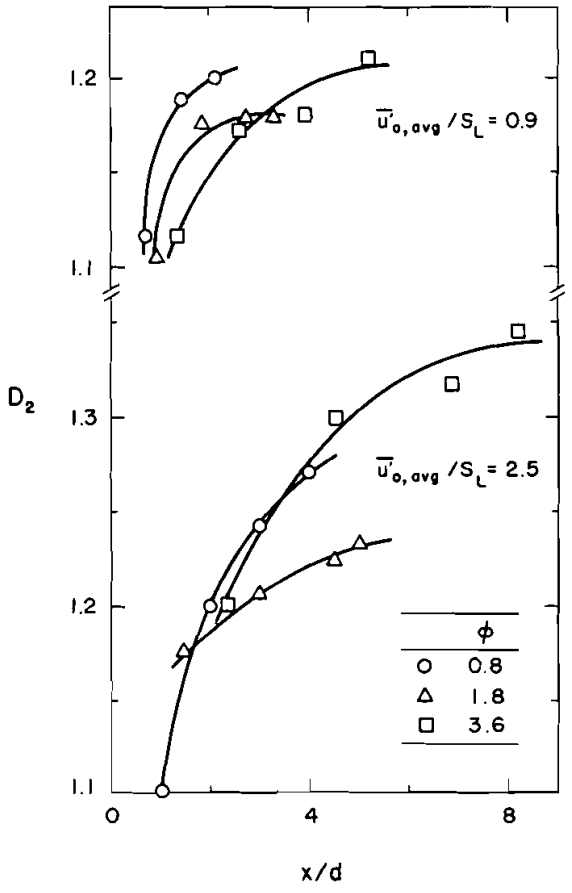

FIGURE 16 Fractal dimension, D_2, for horizontal planes as a function of height above the burner.

increases with increasing distance from the burner. Murayama and Takeno (1988) report similar behavior for D_2 found from horizontal light sheet photographs for lean methane/air turbulent jet flames. Near the burner exit, D_2 approaches unity, which is the value representative of a smooth geometrical surface (Mandelbrot, 1982). This follows since the point of attachment of the flame is fixed along the periphery of the burner passage exit and the turbulence does not have sufficient distance (time) to distort the flame surface from this boundary condition. With increasing distance from the burner exit, the degree of distortion of the flame surface increases, somewhat analogous to the larger lateral distances reached by fluid particles with increasing distance from a fixed source in a uniform turbulent flow due to turbulent dispersion as noted earlier. This results in increased values of D_2 with height above the burner, analogous to the increases of $\bar{r}'_f$, P_T/P_L and A_T/A_L seen in Figures 11–14, at least until the region of the flame tip is approached. The finite extent of the unburned gas imposes another boundary condition which limits the growth of D_2 so that the largest values of D_2 seen in Figure 16 are generally associated with the longest flames. Unlike $\bar{r}'_f$, however, which tends to decrease as the flame tip boundary condition is approached, D_2 behaves more like P_T/P_L and A_T/A_L which simply exhibit reduced rates of growth near the flame tip (see Figures 11–14). A second factor that limits the

ultimate growth of D_2 involves the maximum levels of distortion of surfaces within turbulent flow fields. Measurements of passive surfaces associated with turbulence, like the turbulent/nonturbulent interface in free shear layers and cloud surfaces, yield values of D_3 in the range 2.3–2.4 (Sreenivasan and Meneveau, 1986; Lovejoy, 1982). Gouldin (1987) suggests that similar maximum values of D_3 are appropriate for premixed turbulent flames when $\bar{u}'/S_L$ is large; in fact, values in the range 2.3–2.4 have been observed at large $\bar{u}'/S_L$ by Mantzaras *et al.* (1989) and North and Santavicca (1990). Notably, results for the longest flame in Figure 16 appear to be approaching similar values if the isotropic approximation $D_3 = 1 + D_2$ is applied, even though this flame is stable and $\bar{u}'_{o,\text{avg}}/S_L$ is only 2.5.

The main effect of $\bar{u}'_{o,\text{avg}}/S_L$ on D_2 seen in Figure 16 is that small values of this parameter result in shorter flame lengths for present test conditions which limits the maximum values that D_2 can achieve. Other trends with respect to $\bar{u}'_{o,\text{avg}}/S_L$ alone tend to be obscurred by limited experimental accuracy and effects of preferential diffusion.

Effects of preferential diffusion are quite evident from the results plotted in Figure 16. The effect is most readily seen for $\bar{u}'_{o,\text{avg}}/S_L = 0.9$ where the initial rate of growth of D_2 is much more rapid for $\phi = 0.8$ (unstable) than for $\phi = 3.6$ (stable). Nevertheless, effects of distance from the burner exit also play a role and values of D_2 near the flame tip are actually larger for the longer stable flame than for the unstable flame. Differences between initial growth rates for $\phi = 0.8$ and 3.6 are smaller for $\bar{u}'_{o,\text{avg}}/S_L = 2.5$ than 0.9 but the unstable flame still exhibits higher initial growth rates. Nevertheless, as noted earlier, the long stable flame eventually exhibits the highest values of D_2 observed during present measurements—reaching values expected for passive surfaces in turbulent flows.

Surface Length Scales Measures of flame surface distortion like P_T/P_L, A_T/A_L and D_2 are of interest but it is difficult to relate these quantities to the characteristic scales of the turbulence that are the major factors causing the distortion. As noted earlier, present measurements did not yield useful inner and outer fractal scales: the outer scales were largely fixed by the burner size in the region that could be measured while the inner scales were comparable to present limits of spatial resolution. As an alternative, a flame surface scale or wrinkled wavelength, λ_P, was defined as the wavelength of a square wave that has the same perimeter and r.m.s. fluctuation as the measured flame surface. By calculating the perimeter of a rectangular wave, it is easily shown that

$$\lambda_P = 4\bar{r}'_f/(P_T/P_L - 1). \tag{5}$$

Then using the values of $\bar{r}'_f$ and P_T/P_L plotted in Figures 11–13, the values of λ_P were found. The resulting values of λ_P/l_{uo} are plotted as a function of x/d in Figure 17 for all six flames tested.

In general, wrinkle wavelengths illustrated in Figure 17 are comparable to the integral scale of the turbulence within the unburned gas. Wrinkle wavelengths also decrease with increasing $\bar{u}'_{o,\text{avg}}/S_L$, indicating a finer degree of wrinkling of the flame surface as effects of turbulence begin to dominate the combustion process. Effects of flame position are more complex due to the boundary conditions, with λ_P/l_{uo} increasing near the burner exit and then tending to decrease again as the flame tip is approached. The initial growth is due to development of flame surface distortion, since some distance is required to complete large scale deflections. The final reduction near the flame tip is caused by the reduced size of the region containing unburned gas which limits the scale of the largest distortions. Effects of preferential diffusion can be

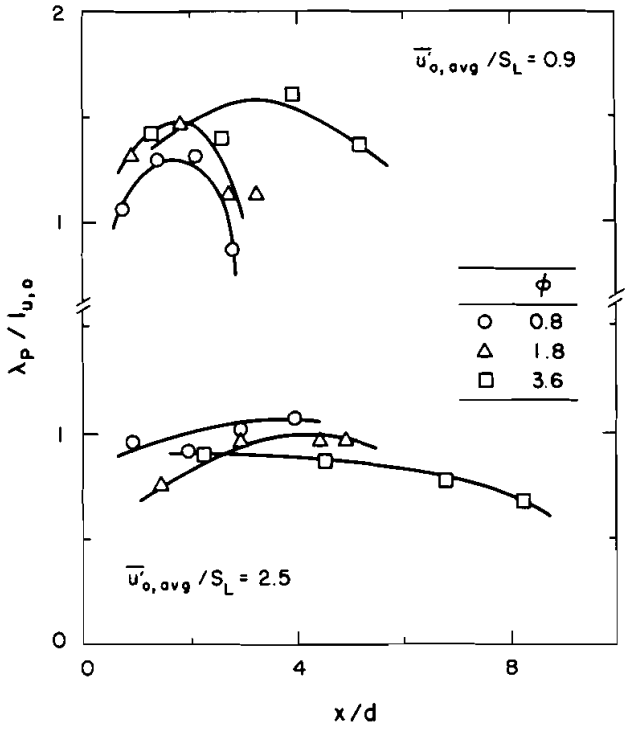

FIGURE 17 Wavelength of flame wrinkles as a function of height above the burner.

seen at $\bar{u}'_{o,avg}/S_L = 0.9$, where $\lambda_P/l_{\omega o}$ is generally smaller for the unstable than the stable flame, reflecting the growth/damping of small-scale disturbances for unstable/stable conditions. However, these trends are not apparent at $\bar{u}'_{o,avg}/S_L = 2.5$ where effects of preferential diffusion are smaller and are obscurred by experimental uncertainties.

DISCUSSION

The conditions of present observations of flame surface properties involved relatively uniform turbulence properties of the unburned gas. Thus, flame sheet properties were largely the result of distortion of the flame surface by a nearly uniform turbulence field. Additionally, present test conditions are far from extinction conditions with relatively high laminar flame speeds and laminar flame thicknesses that are comparable or somewhat smaller than Kolmogorov scales based on reactant gas properties. Thus, effects of local flame stretch (or curvature) mostly influence preferential diffusion (which is absent for neutral conditions) rather than cause local quenching.

The main features of the present observations involve effects of evolution of the distortion of the flame surface with distance from the burner exit, $\bar{u}'_{o,avg}/S_L$, preferential diffusion, and the implications of these phenomena on models of premixed turbulent flames. Effects of flame surface evolution are best considered for neutral conditions where S_T/S_L is proportional to A_T/A_L (Gouldin, 1987). Present results show that A_T/A_L is strongly affected by the geometry of the flame through the boundary conditions: A_T/A_L increases with increasing distance from the burner exit with maximum values largely governed by the length of the flame. The relative

turbulence intensity, $\bar{u}'_{o,avg}/S_L$ primarily affects the initial rate of growth of A_T/A_L. Thus, general correlations between S_T/S_L and $\bar{u}'/S_L$ cannot be expected for turbulent jet flames because the simple expedient of increasing the burner diameter would increase the flame length and accordingly the maximum values of A_T/A_L and S_T/S_L. This behavior is quite plausible at the limit of large $\bar{u}'/S_L$ where the flame surface is similar to an isoproperty surface within a turbulent field (Gouldin, 1987). In these circumstances, turbulent dispersion is well known to increase the lateral spread of tagged fluid particles with increasing distance from the source, leading to a corresponding increase of A_T/A_L. Similarly, flames ignited from a source in a turbulent field undergo progressive development of distortion as they propagate. Thus, while $\bar{u}'/S_L$ influences the rate of increase of A_T/A_L, all flames have large degrees of surface distortion at large distances from the source. As a result, correlations of S_T/S_L solely as a function of $\bar{u}'/S_L$ are only successful to the extent that the rate of growth of A_T/A_L is affected by $\bar{u}'/S_L$ and the fact thay they generally involve a limited range of flame sizes. Much of the scatter seen in plots of this type can probably be attributed to effects of the distance from the point of attachment or ignition to the point where the measurements were made. Notably, recent measurements of Trautwein *et al.* (1990), where the correlation specifically highlights information on distance from the flame source, illustrates this point quite well. In particular, S_T/S_L exhibits a progressive increase with increasing flame size at the time of measurement, analogous to effects of distance from the burner exit observed here. This implies that models of turbulent premixed flames based solely on local conditions, ignoring effects of boundary conditions and distance or time of propagation, are intrinsically incomplete. Thus, premixed turbulent flames are invariably geometry specific, similar to nonpremixed flames which have always been treated as geometry specific.

The same properties of flow development carry over to other parameters of the flame surface like D_2, $\bar{F}'_f$, and λ_P; therefore, present findings concerning these properties are only pertinent for similar flame conditions. Again limiting considerations to neutral conditions, a finite relative velocity of a fluid point with respect to the flow, like S_L, influences the rate of development of flame surface distortion but eventually the degree of distortion must become large just like distances between fluid particles during turbulent dispersion. This implies that the fractal dimension, D_2, must eventually approach values characteristic of isoproperty surfaces in turbulent fields. Indeed, the longest flame studied here eventually approached $D_2 = 1.35$ which is within the range expected, 1.3–1.4, based on past measurements for passive conditions (Lovejoy, 1982; Sreenevasan and Meneveau, 1986). Thus, correlations of D_2 solely as a function of $\bar{u}'/S_L$, like those reported by Mantzaras *et al.* (1989) and North and Santavicca (1990), are only appropriate for a particular time from ignition or distance from a stabilization point. The scatter seen in correlations of this type is probably partly due to effects of flame development, except as the limiting range of D_2 is approached. Certainly, present measurements of D_2 over the six flames would measurably add to the scatter of the plots due to a somewhat different range of flame sizes and the progressive increase of D_2 from values near unity at the burner exit, see Figure 16. Thus, in the absence of a successful method for computing the evolution of D_2, application of fractals to estimate turbulent flame speeds is most appropriate for conditions where D_2 is in the limiting range 1.3–1.4, as originally proposed by Gouldin (1987). Similarly, the largest scales of flame distortion are not fundamentally comparable to integral scales, as has been suggested in previous theories (Shchelkin, 1943), any more than the largest separation distances between fluid particles undergoing turbulent dispersion are limited to integral scales (Hinze, 1975).

Effects of preferential diffusion add another level of complexity to the behavior of

premixed turbulent flames. Present results, and the companion study of Wu *et al.* (1990), demonstrate unequivocally that preferential diffusion is a factor that influences turbulent flame speeds and the rate of development of turbulent distortion of the flame surface at Reynolds numbers of interest for practical applications. The effect is to reduce/increase the rate of increase of flame distortion for stable/unstable conditions, similar to the predictions of Clavin and Williams (1979, 1982) for premixed flames in weak turbulence. When preferential diffusion effects are present, direct proportionality between S_T/S_L and A_T/A_L is questionable (Gouldin, 1987); nevertheless, existing observations suggest that this correspondence is at least roughly correct. Recognizing this and the fact that correlations of S_T/S_L as a function of $\bar{u}'/S_L$ for particular test conditions largely reflect the rate of growth of flame distortion, several other studies support present findings. For example, Abdel-Gayed *et al.* (1976, 1984) and Wu *et al.* (1990) observe higher values of S_T/S_L at particular values of $\bar{u}'/S_L$ for lean (unstable) than rich (stable) hydrogen/air flames. Liu and Lenze (1988) report similar findings for flames involving CH_4–H_2 mixtures and air. Finally, Abdel-Gayed *et al.* (1984) find higher values of S_T/S_L at a given $\bar{u}'/S_L$ for rich (unstable) than lean (stable) propane/air and iso-octane/air flames. The last observations are of particular interest because many practical premixed turbulent flames, like those in spark-ignition engines, involve heavy hydrocarbons burning in air at lean (stable) conditions where effects of preferential diffusion can significantly retard the rate of growth of distortion of the flame surface.

Taken together, effects of the development of flame surface distortion and preferential diffusion preclude the effective use of premixed turbulent combustion models that are based solely on local conditions and only involve passive propagation of the flame at a fixed laminar flame speed with respect to the unburned gas. A possible exception involves mixing controlled neutral stability conditions where D_2 is in the range appropriate for isoproperty surfaces in turbulent fields and $\bar{u}'/S_L$ is small (Bray, 1980; Goulding, 1987; Wu *et al.*, 1990). Thus, because practical applications meeting the criteria of the exceptions are limited, while existing models and correlations of premixed turbulent flame phenomena are generally incomplete with respect to flame development and preferential diffusion, past ideas concerning models and correlations of turbulent premixed flame processes should be re-examined.

CONCLUSIONS

The major conclusions of the study can be summarized as follows:

1. Spatial variations of flame surface properties were quantified. As the distance from the flameholder increased, even though unburned gas turbulence properties were relatively constant, the following properties increased in value: flame surface area (and thus the local turbulent burning velocity), flame brush thickness and the fractal dimension of the flame surface. Approach to the flame tip limits the maximum value of these properties. Thus, effects of the attachment and flame tip boundary conditions imply that turbulent premixed flames are geometry specific while the spatial variations imply that models or correlations of turbulent flame properties based on local properties alone, and don't specifically account for distance from the flameholder, are intrinsically incomplete.
2. Increasing values of $\bar{u}'/S_L$ tend to increase the rate of turbulent distortion of the flame surface with distance from the flameholder and also increase levels of fine-grained roughness of the flame surface. Thus correlations of S_T/S_L solely as a function of $\bar{u}'/S_L$ can be found because they reflect this rate of increase over

limited ranges of flame dimensions. Nevertheless, such correlations are incomplete unless they account for development of flame surface properties with distance from the flameholder (or point of ignition).

3. Effects of preferential diffusion were significant even at the high Reynolds numbers of present experiments, acting to reduce/increase the rate of flame distortion (and correspondingly the local turbulent velocity) for stable/unstable conditions. Review of earlier work in the literature revealed that this behavior is not limited to the present hydrogen/air flames due to the unusually large mass diffusivity of hydrogen, *e.g.*, similar behavior has been observed for methane, propane and iso-octane/air flames (Abdel-Gayed *et al.*, 1976, 1984; Liu and Lenze, 1988). In particular, spark ignition engines use mixtures of heavy hydrocarbons and air and operate fuel lean; this places then in stable preferential diffusion conditions which should retard the rate of development of flame surface distortion. Few practical applications involve neutral preferential diffusion conditions; therefore, models and correlations of premixed flame properties should be re-examined to consider effects of preferential diffusion that are important for both stable and unstable conditions. Exceptions may be found at large $\bar{u}'/S_L$ and distances from the flameholder where effects of preferential diffusion tend to decrease, however, additional study is needed to confirm this trend.
4. Measurements showed that the turbulence properties of the unburned gas were relatively uniform and did not change appreciably as the flame surface was approached. Present measurements include findings for stable, neutral and unstable preferential diffusion conditions (with nearly identical burner exit conditions and laminar flame speeds for stable and unstable conditions), various values of $\bar{u}'_{o,\mathrm{avg}}/S_L$, and a reasonably complete characterization of unburned gas properties. Coupled with current understanding of the structure of laminar hydrogen/air flames, it is hoped that this information will prove to be useful for developing more complete models and correlations of the properties of premixed turbulent combustion processes than now exist.

ACKNOWLEDGEMENTS

This research was supported by the Office of Naval Research, Contract No. N00014-87-K-0698, with S. Ramberg serving as Scientific Program Officer.

REFERENCES

Abdel-Gayed, R. G., and Bradley, D. (1976). Dependence of turbulent burning velocity on turbulent Reynolds number and ratio of laminar burning velocity to r.m.s. turbulent velocity. *Sixteenth Symposium (International) on Combustion*, The Combustion Institute, Pittsburgh, pp. 1725–1735.

Abdel-Gayed, R. G., Bradley, D., Hamid, M. M., and Lawes, M. (1984). Lewis number effects on turbulent burning velocity. *Twentieth Symposium (International) on Combustion*, The Combustion Institute, Pittsburgh, pp. 505–512.

Andrews, G. E., and Bradley, D. (1973). Determination of burning velocity by double ignition in a closed vessel. *Combust. Flame*, **20**, 77.

Ballal, D. R. (1979). The structure of a premixed turbulent flame. *Proc. R. Soc. London* **A367**, 353.

Box, G. P., and Jenkins, G. M. (1976). *Time Series Analysis*, Holden-Day, San Francisco, CA, pp. 47–66.

Boyer, L., Clavin, P., and Sabathier, F. (1980). Dynamic behavior of a premixed turbulent flame front. *Eighteenth Symposium (International) on Combustion*, The Combustion Institute, Pittsburgh, pp. 1041–1049.

Bray, K. N. C. (1980). Turbulent flows with premixed reactants. In P. A. Libby and F. A. Williams (Eds.), *Turbulent Reacting Flows*, Springer, Berlin, pp. 115–183.

Cant, R. S., and Bray, K. N. C. (1988). Strained laminar flamelet calculations of premixed turbulent combustion in a closed vessel. *Twenty-Second Symposium (International) on Combustion*, The Combustion Institute, Pittsburgh, pp. 791–799.

Clavin, P. (1985). Dynamic behavior of premixed flame fronts in laminar and turbulent flows. *Prog. Energy Combust. Sci.*, **11**, 1.

Clavin, P., and Williams, F. A. (1979). Theory of premixed-flame propagation in large-scale turbulence. *J. Fluid Mech.*, **90**, 589.

Clavin, P., and Williams, F. A. (1982). Effects of molecular diffusion and of thermal expansion in the structure and dynamics of premixed flames in turbulent flows of large scale and low intensity. *J. Fluid Mech.*, **116**, 251.

Gouldin, F. C. (1987). An application of fractals to modeling premixed turbulent flames. *Combust. Flame*, **68**, 249.

Gouldin, F. C., Hilton, S. M., and Lamb, T. (1988). Experimental evaluation of the fractal geometry of flamelets. *Twenty-Second Symposium (International) on Combustion*, The Combustion Institute, Pittsburgh, pp. 541–550.

Grover, J. H., Fales, E., and Scurlock, A. C. (1959). Turbulent flame studies in a two-dimensional open burner. *ARS J.*, **26**, 275.

Hinze, J. O. (1975). *Turbulence*, McGraw-Hill, New York, 2nd edition, Chapt. 4.

Incropera, F. P., and DeWitt, D.P. (1981). *Fundamentals of Heat Transfer*, John Wiley & Sons, New York, p. 785.

Joulin, G., and Mitani, T. (1981). Linear stability analysis of two-reactant flames. *Combust. Flame*, **40**, 235.

Laufer, J. (1954). Cited in Hinze, J. O. (1975). *Turbulence*, McGraw-Hill, New York, 2nd edition, pp. 720–724.

Libby, P. A., Sivasegaram, S., and Whitelaw, J. H. (1986). Premixed combustion. *Prog. Energy Combust. Sci.*, **12**, 353.

Liu, Y., and Lenze, B. (1988). The influence of turbulence on the burning velocity of premixed CH_4-H_2 flames with different laminar burning velocities. *Twenty-Second Symposium (International) on Combustion*, The Combustion Institute, Pittsburgh, pp. 747–754.

Lovejoy, S. (1982). Area-perimeter relation for rain and cloud areas. *Science*, **216**, 185.

Mandelbrot, B. B. (1982). *The Fractal Geometry of Nature*, W. H. Freeman, San Francisco.

Manton, J., von Elbe, G., and Lewis, B. (1952). Nonisotropic propagation of combustion waves in explosive gas mixtures and development of cellular flames. *J. Chem. Phys.*, **20**, 153.

Mantzaras, J., Felton, P. G., and Bracco, F. V. (1989). Fractals and turbulent premixed engine flames. *Combust. Flame*, **77**, 295.

Murayama, M., and Takeno, T. (1988). Fractal-like character of flamelets in turbulent combustion. *Twenty-Second Symposium (International) on Combustion*, The Combustion Institute, Pittsburgh, pp. 551–559.

Nikuradse, J. (1932). Cited in Hinze, J. O. (1975), McGraw-Hill, New York, 2nd edition, pp. 725–727.

North, G. L., and Santavicca, D. A. (1990). The fractal nature of premixed turbulent flames. *Combust. Sci. and Tech.*, in press.

Peters, N. (1986). Laminar flamelet concepts in turbulent combustion. *Twenty-First Symposium (International) on Combustion*, The Combustion Institute, Pittsburgh, pp. 1231–1250.

Pope, S. B. (1990). Computations of turbulent combustion: progress and challenges. *Twenty-Third Symposium (International) on Combustion*, The Combustion Institute, Pittsburgh, in press.

Santavicca, D. A., Liou, D., and North, G. L. (1990). A fractal model of turbulent flame kernal growth. SAE Paper No. 900024.

Searby, G., and Clavin, P. (1986). Weakly turbulent, wrinkled flames in premixed gases. *Combust. Sci. and Tech.*, **46**, 167.

Shchelkin, K. I. (1943). Cited in Lewis, B., and von Elbe, G. (1961). *Combustion, Flames and Explosions in Gases*, Academic Press, New York, 2nd edition, Section 6.3.

Sreenivasan, K. R., and Meneveau, C. (1986). The fractal facets of turbulence. *J. Fluid Mech.*, **173**, 357.

Tennekes, H., and Lumley J. L. (1972). *Turbulence*, M.I.T. Press, Cambridge, MA, pp. 67.

Trautwein, S. E., Grudno, A., and Adomeit, G. (1990). The influence of turbulence intensity and laminar flame speed on turbulent flame propagation under engine like conditions. *Twenty-Third Symposium (International) on Combustion*, The Combustion Institute, Pittsburgh, in press.

Videto, B. D., and Santavicca, D. A. (1990). Flame-turbulence interactions in a freely-propagating, premixed flame. *Combust. Sci. and Tech.*, in press.

Williams, F. A. (1985). *Combustion Theory*, Benjamin/Cummings, Menlo Park, CA, 2nd edition, pp. 341–372, 411–445.

Wu, M.-S., Kwon, S., Driscoll, J. F., and Faeth, G. M. (1990). Turbulent premixed hydrogen/air flames at high Reynolds numbers. *Combust. Sci. and Tech.*, **73**, 327.